Effective axial-vector strength within proton-neutron deformed quasiparticle random-phase approximation

D. S. Delion,[1,2,3] A. Dumitrescu,[1,2] and J. Suhonen[4]

[1] *"Horia Hulubei" National Institute of Physics and Nuclear Engineering, 30 Reactorului, RO-077125 Bucharest-Măgurele, România*

[2] *Academy of Romanian Scientists, 54 Splaiul Independenţei, RO-050094 Bucharest, România*

[3] *Bioterra University, 81 Gârlei, RO-013724 Bucharest, România*

[4] *Department of Physics, University of Jyväskylä, P.O. Box 35 (YFL), FI-40014 Jyväskylä, Finland*

(Received 14 May 2019; revised manuscript received 9 July 2019; published 26 August 2019)

We use the available experimental Gamow-Teller β^- and β^+/EC (electron-capture) decay rates between 0^+ and 1^+ ground states in neighboring even-even and odd-odd nuclei, combined with $2\nu\beta\beta$ half-lives, to analyze the influence of the nuclear environment on the weak axial-vector strength $g_{\rm A}$. For this purpose, the proton-neutron deformed quasiparticle random-phase approximation (pn-dQRPA), with schematic dipole residual interaction is employed. The Hamiltonian contains particle-hole (ph) and particle-particle (pp) channels with mass-dependent strengths. In deriving the equations of motion we use a self-consistent procedure in terms of a single-particle basis with projected angular momentum provided by the diagonalization of a spherical mean field plus the quadrupole-quadrupole interaction. Our analysis evidenced a quenched average effective value $\langle g_{\rm A}\rangle \approx 0.7$ with a root-mean-square deviation of $\sigma \approx 0.3$ for transitions from even-even emitters and $\sigma \approx 0.6$ for transitions from odd-odd emitters.

DOI: 10.1103/PhysRevC.100.024331

I. INTRODUCTION

One of the central topics in modern subatomic physics is the investigation of nuclear double-beta ($\beta\beta$) decay processes [1,2]. The neutrinoless double-beta $0\nu\beta\beta$ decay, not yet experimentally detected, is particularly important when exploring physics beyond the standard-model connected to the fundamental nature of the neutrino. The basic problem is to relate the nuclear matrix elements (NMEs) entering nuclear many-body calculations to the neutrino properties [3]. At present there are several models describing double-beta decay in medium-heavy and heavy nuclei [4–7].

A major issue is the unknown effective value of the weak axial-vector coupling strength $g_{\rm A}$ entering the $0\nu\beta\beta$-decay amplitude as $g_{\rm A}^2$ and the decay half-life as $g_{\rm A}^{-4}$. This problem is similar to the use of an effective charge to describe electromagnetic excitations in nuclei. The first studies of $g_{\rm A}$ in the context of $2\nu\beta\beta$ decays were performed in Ref. [8] by using the microscopic interacting boson model (IBM-2). There, strongly quenched effective values were obtained, in the range $g_{\rm A} \approx 0.5$. Similar values were also obtained in earlier shell-model (SM) studies of Gamow-Teller (GT) β decays, as in Refs. [9,10]. Even earlier, simultaneous studies of GT β and $2\nu\beta\beta$ decays were done to probe the effective value of $g_{\rm A}$. The first investigation was performed in Ref. [11], using the spherical proton-neutron quasiparticle random-phase approximation (pn-QRPA) to describe the β and $2\nu\beta\beta$ decays in the $A = 100, 116$ isobaric triplets with an effective value of $g_{\rm A}$. A similar study in the $A = 100, 116, 128$ isobaric triplets was later performed in Ref. [12] and close effective values of $g_{\rm A}$ were obtained for the β [$g_{\rm A}(\beta)$] and $2\nu\beta\beta$ [$g_{\rm A}(\beta\beta)$] decays. Recently, in Ref. [13], the $A = 128, 130$ isobaric triplets were investigated within the interacting boson-fermion-fermion model (IBFFM-2). An up-to-date review concerning various systematics of the effective axial-vector strength is given in Table 3 of Ref. [14].

A common outcome of these studies is the relatively large scattering of $g_{\rm A}$ values, in the range $g_{\rm A} \approx 0.25$–0.82. In particular, the obtained range based on β decays is $g_{\rm A}(\beta) \approx 0.25$–$0.71$. Let us mention that the extracted effective value of $g_{\rm A}$ depends on the adopted nuclear many-body framework, such as IBM-2, IBFFM-2, pn-QRPA, SM, etc. (see Ref. [14] for details). There are also several other sources that affect the value of $g_{\rm A}$, as shown in Refs. [15,16].

The traditionally employed microscopic model for $\beta\beta$-decay calculations is the pn-QRPA [17]. Mostly the pnQRPA based on a spherical mean field has been used in calculations. However, many β and $\beta\beta$ decaying nuclei are more or less deformed and therefore it is very important to extend the description to a deformed mean field. This is the starting point of the deformed pn-QRPA (pn-dQRPA). Most of the earlier approaches describe GT beta decays by using a pn-dQRPA phonon in the intrinsic system of coordinates, i.e., in terms of pairs of Nilsson quasiparticles coupled to a $K = 1$ spin projection. The physical observables, such as β-decay transition probabilities, are then estimated by rotating the intrinsic phonon to the laboratory system of coordinates [18,19]. This formalism was applied in the attempt to describe 1^+ GT states and $2\nu\beta\beta$ decays in several papers [20–25]. We stress one important point, namely that this projection procedure restores only the symmetry of the phonon by leaving the pn-dQRPA ground state deformed. A more consistent approach is to use a single-particle (sp) basis with good angular momentum directly in the derivation of the pn-dQRPA equations.

One way to obtain this basis consists in projecting good angular momentum from the product between a coherent state, describing the deformed core, and a spherical sp state [26]. The pn-dQRPA phonon, describing GT β decays, is built by using pairs of these quasiparticles that are "dressed by deformation" and coupled to the spin $J = 1$ [27,28]. Later on, in Ref. [29], this approach was generalized by considering all allowed spherical sp states in order to build a sp state "dressed by deformation." A particular case is the adiabatic limit, which is nothing else than the usual Nilsson wave function expressed in the laboratory frame. We successfully described the available experimental $B(E2)$ values for collective states in the range $50 \leqslant Z \leqslant 100$ in even-even nuclei by using the adiabatic version of this formalism [29]. Later on we described $2\nu\beta\beta$ decays within the proton-neutron version of dQRPA (pn-dQRPA) in Ref. [30].

In the present work we use the pn-dQRPA to generalize our earlier results [31] on the problem of the effective axial-vector strength by using the available data on GT β^- and β^+/EC (electron-capture) decay rates between 0^+ states in even-even and 1^+ states in neighboring odd-odd nuclei. It turns out that an additional analysis of $2\nu\beta\beta$ half-lives is essential for determining the effective value of $g_{\rm A}$.

The paper is organized according to the following scheme: in Sec. II we describe the theoretical framework of pn-dQRPA, in Sec. III we analyze the experimental data, and in the last section we draw conclusions.

II. THEORETICAL BACKGROUND

In order to describe the 1^+ GT states in odd-odd deformed nuclei, we proceed with the steps described in Refs. [30,32].

(1) We first build a deformed sp basis with good angular momentum starting from the standard Nilsson sp representation in the intrinsic frame, which is then transformed in the laboratory system of coordinates [29]:

$$\begin{aligned} |\tau\, jm) &= a^\dagger_{\tau\, jm}(\Omega)|0) \\ &= \sum_{J=\text{even}} \sum_{j_s \geqslant j} \mathcal{X}^{Jk_s}_{\tau j} [Y_J(\Omega) \otimes |\tau k_s\rangle]_{jm}, \\ |\tau k_s \nu\rangle &= c^\dagger_{\tau k_s \nu}|0\rangle, \quad \tau = p, n, \end{aligned} \tag{2.1}$$

where Ω denotes the Euler angles of the intrinsic symmetry axis with respect to the laboratory system and $j \equiv (\epsilon, j^\pi)$ (deformed eigenvalue, total spin$^{\text{parity}}$). The creation operators $c^\dagger_{\tau k_s \nu}$ describe the eigenstates of a spherical nuclear plus proton Coulomb mean field having the quantum numbers $k_s \equiv (e, l, j_s)$ (spherical eigenvalue, orbital angular momentum, total spherical spin), with ν being the z projection of j_s. The expansion coefficients are proportional to standard Nilsson amplitudes with $j = K$, where K is the spin projection on the intrinsic symmetry axis:

$$\mathcal{X}^{Jk_s}_{\tau j} = \sqrt{2}\langle jj; j_s - j|J0\rangle x^{k_s}_{\tau j}, \tag{2.2}$$

and by the bra-ket product we denoted the Clebsch-Gordan coefficient. The amplitudes $x^{k_s}_{\tau j}$ in Eq. (2.2) are found by diagonalizing the quadrupole-quadrupole (QQ) operator in the spherical Woods-Saxon basis. Let us mention that both the $\mathcal{X}$ and x amplitudes satisfy orthonormality relations. Notice that in the spherical limit, where one has $x^{k_s}_{\tau j} = \delta_{j_s j}$, the operator (2.1) is proportional to the usual spherical sp creation operator with a "statistical" coefficient

$$\mathcal{X}^{Jk_s}_{\tau j} = \sqrt{\frac{2}{2j+1}}\delta_{j_s j}, \tag{2.3}$$

expressing the fact that two particles with intrinsic projections $K = \pm j$ are distributed over $2j + 1$ projections in the laboratory system of coordinates.

The particular case of laboratory sp amplitudes given by Eq. (2.2) is what we call "adiabatic approach," because we used the standard intrinsic Nilsson wave function with components x, having a given intrinsic angular momentum projection, but "seen" in the laboratory frame according to the relation (2.1). Thus, the Coriolis mixing of angular momentum projections is neglected. In the general case, the amplitudes $\mathcal{X}$ entering Eq. (2.1) can be obtained by diagonalizing the QQ interaction directly in the laboratory frame. This is of course a trivial operation, but unfortunately the particle occupancy of the obtained sp levels implies a more involved rule than two particles/level and, for instance, a quasiparticle is built in terms of all sp components instead of two time-reversed states defined later by Eq. (2.9). Anyway, our analysis concerning $B(E2)$ values in well deformed nuclei [29] showed that the so-called adiabatic approach gives very good results. For this reason we also used this simplification in the analysis of beta decays.

(2) The one-body particle-hole (ph) operators in this representation are given by

$$Q_{\lambda\mu} = \sum_{j_1 j_2} \frac{(\tau_1 j_1 ||Q_\lambda||\tau_2 j_2)}{\widehat{\lambda}} [a^\dagger_{\tau_1 j_1} \otimes \tilde{a}_{\tau_2 j_2}]_{\lambda\mu}, \tag{2.4}$$

where we dropped the Euler angles Ω for simplicity. The reduced matrix element in the deformed basis (2.1) is given by integration over Euler angles

$$\begin{aligned} (\tau_1 j_1 ||Q_\lambda||\tau_2 j_2) = \widehat{j_1}\widehat{j_2} \sum_{Jk_{s1}k_{s2}} & \mathcal{X}^{Jk_{s1}}_{\tau_1 j_1} \mathcal{X}^{Jk_{s2}}_{\tau_2 j_2} \\ & \times (-)^{j_{s1}+j_2+\lambda-J} W(j_1 j_{s1} j_2 j_{s2}; J\lambda) \\ & \times \langle \tau_1 k_{s1}||Q_\lambda||\tau_2 k_{s2}\rangle, \end{aligned} \tag{2.5}$$

where $\widehat{j} = \sqrt{2j+1}$ and W is the Racah coefficient. One has a similar result for a particle-particle (pp) operator. For the monopole particle-number and pairing operators in the laboratory system we will consider the leading $J = 0$ component:

$$\begin{aligned} N_{\tau j} &\approx \left(x^j_{\tau j}\right)^2 \frac{2}{2j+1} \sum_m a^\dagger_{\tau jm} a_{\tau jm}, \\ P^\dagger_{\tau j} &\approx \left(x^j_{\tau j}\right)^2 \frac{2}{2j+1} \sum_m a^\dagger_{\tau jm} a^\dagger_{\tau j-m} (-)^{j-m}. \end{aligned} \tag{2.6}$$

We use a monopole pairing plus a separable proton-neutron interaction with constant strengths in both the ph and pp

channels:

$$H = \sum_p (\epsilon_p - \lambda^{\rm prot}) N_p - \frac{G^{\rm prot}_{\rm pair}}{4} \sum_{pp'} P^\dagger_p P_{p'} + \sum_n (\epsilon_n - \lambda^{\rm neut}) N_n - \frac{G^{\rm neut}_{\rm pair}}{4} \sum_{nn'} P^\dagger_n P_{n'} + g_{\rm ph} \sum_\mu D^-_{1\mu} (D^-_{1\mu})^\dagger - g_{\rm pp} \sum_\mu P^-_{1\mu} (P^-_{1\mu})^\dagger, \quad (2.7)$$

where the meaning of the shorthand notation is $\tau \equiv (\tau, \epsilon j^\pi)$. Here, the chemical potential for protons (neutrons) is denoted by $\lambda^{\rm prot}$ ($\lambda^{\rm neut}$). The strength parameters $g_{\rm ph}$ (particle-hole) and $g_{\rm pp}$ (particle-particle) are the ones of the corresponding spherical limit in Refs. [33,34], and are given in units of MeV.

The GT operators are given by

$$D^-_{1\mu} = \frac{1}{\sqrt{3}} \sum_{pn} (p||\sigma||n)[a^\dagger_p \otimes \tilde{a}_n]_{1\mu}, \qquad P^-_{1\mu} = \frac{1}{\sqrt{3}} \sum_{pn} (p||\sigma||n)[a^\dagger_p \otimes a^\dagger_n]_{1\mu}, \quad (2.8)$$

in terms of the Pauli operator σ_μ. The reduced matrix element in the deformed basis (2.1) is given in terms of the standard spherical matrix element by Eq. (2.5) with $\lambda = 1$.

(3) The next step involves introducing a quasiparticle representation for protons and neutrons:

$$a^\dagger_{\tau m} = u_\tau \alpha^\dagger_{\tau m} + v_\tau \alpha_{\tau -m} (-)^{j_\tau - m}, \quad \tau = p, n, \quad (2.9)$$

where u and v are the BCS vacancy and occupation amplitudes respectively. These are used to obtain the β-decay operators entering the Hamiltonian (2.7). The BCS equations have formally the structure of the deformed case due to the "statistical" factors entering the particle-number and pairing operators (2.6). By using the quasiparticle representation (2.9) one obtains

$$D^-_{1\mu} = \sum_{pn} [\xi_{pn} A^\dagger_{1\mu}(pn) + \bar{\xi}_{pn} A_{1-\mu}(pn)(-)^{1-\mu}], \qquad P^-_{1\mu} = \sum [\eta_{pn} A^\dagger_{1\mu}(pn) - \zeta_{pn} A_{1-\mu}(pn)(-)^{1-\mu}], \quad (2.10)$$

where

$$A^\dagger_{1\mu}(pn) = [\alpha^\dagger_p \otimes \alpha^\dagger_n]_{1\mu} = (-)^{j_p + j_n} A^\dagger_{1\mu}(np), \qquad A_{1\mu}(pn) = (A^\dagger_{1\mu}(pn))^\dagger = (-)^{1-\mu} [\tilde{\alpha}_n \otimes \tilde{\alpha}_p]_{1-\mu} \quad (2.11)$$

depend also on the Euler angles Ω, and we have defined

$$\xi_{pn} = \frac{(p||\sigma||n)}{\sqrt{3}} u_p v_n = (-)^{j_p - j_n} \bar{\xi}_{np}, \quad \bar{\xi}_{pn} = \frac{(p||\sigma||n)}{\sqrt{3}} v_p u_n = (-)^{j_p - j_n} \xi_{np}, \quad \eta_{pn} = \frac{(p||\sigma||n)}{\sqrt{3}} u_p u_n = (-)^{j_p - j_n} \eta_{np}, \quad \zeta_{pn} = \frac{(p||\sigma||n)}{\sqrt{3}} v_p v_n = (-)^{j_p - j_n} \zeta_{np}. \quad (2.12)$$

(4) Finally, we diagonalize the proton-neutron interaction within the pn-dQRPA framework by using the phonon

$$\Gamma^\dagger_{1\mu}(\omega) = \sum_{pn} \left[X^\omega_{pn} A^\dagger_{1\mu}(pn) - Y^\omega_{pn} (-)^{1-\mu} A_{1-\mu}(pn) \right], \quad (2.13)$$

given in terms of the creation pair operator (2.11) with ω the eigenvalue index. Using the boson commutation rule

$$\int d\Omega [\Gamma_{1\mu}(\omega), \Gamma^\dagger_{1\mu}(\omega')] = \delta_{\omega,\omega'}, \quad (2.14)$$

one obtains the standard orthonormality condition for amplitudes,

$$\sum_{pn} \left(X^\omega_{pn} X^{\omega'}_{pn} - Y^\omega_{pn} Y^{\omega'}_{pn} \right) = \delta_{\omega,\omega'}. \quad (2.15)$$

The equations of motion are derived from a projection procedure over Euler angles, i.e.,

$$\int d\Omega \left[A_{1\mu}, \left[H, \Gamma^\dagger_{1\mu}(\omega) \right] \right] = \omega \int d\Omega \left[A_{1\mu}, \Gamma^\dagger_{1\mu}(\omega) \right], \quad (2.16)$$

and a similar relation with $A^\dagger_{1-\mu}$. The pn-dQRPA equations of motion,

$$\begin{pmatrix} \mathcal{A}_{pn,p'n'} & \mathcal{B}_{pn,p'n'} \\ -\mathcal{B}_{pn,p'n'} & -\mathcal{A}_{pn,p'n'} \end{pmatrix} \begin{pmatrix} X^\omega_{p'n'} \\ Y^\omega_{p'n'} \end{pmatrix} = \omega \begin{pmatrix} X^\omega_{pn} \\ Y^\omega_{pn} \end{pmatrix}, \quad (2.17)$$

are formally given by the usual spherical relations

$$\mathcal{A}_{pn,p'n'} = \delta_{pp'} \delta_{nn'} (E_p + E_n) + 2 g_{ph} (\xi_{pn} \xi_{p'n'} + \bar{\xi}_{pn} \bar{\xi}_{p'n'}) - 2 g_{pp} (\eta_{pn} \eta_{p'n'} + \zeta_{pn} \zeta_{p'n'}),$$
$$\mathcal{B}_{pn,p'n'} = 2 g_{ph} (\xi_{pn} \bar{\xi}_{p'n'} + \bar{\xi}_{pn} \xi_{p'n'}) + 2 g_{pp} (\eta_{pn} \zeta_{p'n'} + \zeta_{pn} \eta_{p'n'}), \quad (2.18)$$

but in terms of deformed quasiparticle spectra E_p, E_n and reduced matrix elements multiplied by BCS amplitudes (2.12). Thus, in the present approach the QRPA vacuum is spherical, in contrast to the approximations adopted earlier where the spherical symmetry of the phonon was restored after deriving the equations of motion, still leaving the vacuum itself deformed.

We define the GT β-decay transition matrix elements as follows [35]:

$$\beta^-_{\omega 0} = \beta^+_{0\omega} \equiv (\omega||\beta^-||0) = \sqrt{3} \sum_{pn} \left(\xi_{pn} X^\omega_{pn} + \bar{\xi}_{pn} Y^\omega_{pn} \right), \qquad \beta^+_{\omega 0} = \beta^-_{0\omega} \equiv (\omega||\beta^+||0) = \sqrt{3} \sum_{pn} \left(\bar{\xi}_{pn} X^\omega_{pn} + \xi_{pn} Y^\omega_{pn} \right). \quad (2.19)$$

These transitions are described within the pn-dQRPA formalism and they are schematically shown in Fig. 1. We find the eigenvalues ω and amplitudes X, Y by using a standard diagonalization procedure, but let us mention that one can also derive the following analytic expressions for the amplitudes:

$$\begin{pmatrix} X^\omega_{pn} \\ Y^\omega_{pn} \end{pmatrix} = \frac{\xi_{pn} x_1 + \bar{\xi}_{pn} x_2 + \eta_{pn} x_3 + \zeta_{pn} x_4}{E_p + E_n \mp \omega}, \quad (2.20)$$

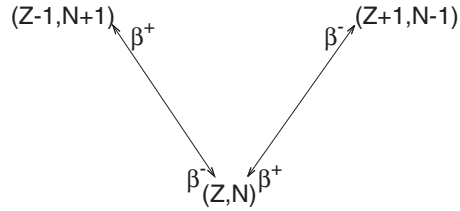

FIG. 1. Weak processes described by the pn-dQRPA.

where the x_k coefficients satisfy a 4×4 homogeneous system of linear equations.

The $2\nu\beta\beta$ double GT matrix element is written as follows [17]:

$$M_{\rm GT} = \sum_{mn} \frac{\langle 0\|\beta^-\|\omega_m^f\rangle\langle\omega_m^f|\omega_n^i\rangle\langle\omega_n^i\|\beta^-\|0\rangle}{D_m}, \qquad (2.21)$$

where the energy denominator is given by

$$D_m = \frac{\frac{1}{2}\left(\Delta_{\rm exp} + \tilde{\omega}_m^i + \tilde{\omega}_m^f\right) + E_{\rm ex}(1_1^+) + \Delta M_i^{\rm exp}}{m_{\rm e}c^2}. \qquad (2.22)$$

Here, $\tilde{\omega}_m = \omega_m - \omega_1$, $\Delta_{\rm exp}$ is the nuclear mass difference between the initial and final states, $E_{\rm ex}(1_1^+)$ is the experimental energy of the first 1^+ state in the intermediate odd-odd nucleus, $\Delta M_i^{\rm exp}$ is the measured difference of the mass energies of the intermediate and initial nuclei, and $m_{\rm e}c^2$ the electron rest mass.

The detailed description of the $2\nu\beta\beta$ transition rate (2.21) is given in Sec. 2.1 of Ref. [17]. In particular, the overlap between the initial 1_n^+ and final 1_m^+ states in this relation, $\langle\omega_m^f|\omega_n^i\rangle$, is given by similar expressions to Eqs. (2.9)– (2.11) of Ref. [23], but using our pn-dQRPA amplitudes:

$$\begin{aligned}\langle\omega_m^f|\omega_n^i\rangle = &\sum_{pn,p'n'} \left[X_{pn}^{\omega_m^f} X_{p'n'}^{\omega_n^i} - Y_{pn}^{\omega_m^f} Y_{p'n'}^{\omega_n^i}\right] \\ &\times \left(u_p^f u_{p'}^i + v_p^f v_{p'}^i\right)\left(u_n^f u_{n'}^i + v_n^f v_{n'}^i\right) \\ &\times \langle p|p'\rangle\langle n|n'\rangle\langle {\rm BCS}_f|{\rm BCS}_i\rangle. \qquad (2.23)\end{aligned}$$

III. NUMERICAL APPLICATION

We analyzed experimental data concerning β^- and β^+/EC transitions from (to) 0^+ ground states of even nuclei to (from) 1^+ ground states of neighboring odd-odd nuclei [36]. We used as spherical sp states $c_{\tau k_s \nu}^\dagger$ the eigenstates of the spherical Woods-Saxon plus proton Coulomb mean field with the universal parametrization of Ref. [37]. The deformed eigenstates $a_{\tau jm}^\dagger$, given by Eq. (2.1), are obtained by diagonalizing the quadrupole-quadrupole interaction in the adiabatic limit, thus neglecting the Coriolis forces. The quadrupole deformation parameters were taken from Ref. [38]. The u_τ and v_τ amplitudes were determined by solving the BCS equations for protons and neutrons with monopole interaction reproducing the experimental pairing gaps. In order to build the pn-dQRPA basis we first ordered the *pn* reduced matrix elements in decreasing order of their magnitude and then used the first 100 *pn* pairs.

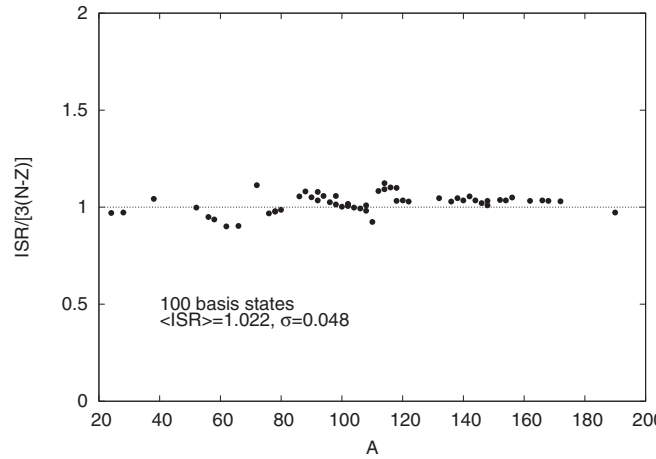

FIG. 2. Ikeda sum rule (3.1) compared to $3(N-Z)$ versus mass number. σ denotes the rms deviation from the mean.

It is known that the so-called Ikeda sum rule,

$$\mathrm{ISR} = \sum_\omega [(\beta_{\omega 0}^-)^2 - (\beta_{\omega 0}^+)^2] = 3(N-Z), \qquad (3.1)$$

is automatically fulfilled within the spherical pn-QRPA [35]. In order to check the accuracy of the rule in our case, we use in this relation the transition operators given by the deformed approach (2.19). In Fig. 2 we plot the ratio $\mathrm{ISR}/[3(N-Z)]$ against the mass number A. One sees that the rule is reasonably fulfilled with a mean value of 1.02 and an overall deviation of less than 5%. Let us mention that in the standard pn-QRPA the Ikeda sum rule is saturated by increasing the number of basis states. In this case the Ikeda sum rule (ISR) can be analytically derived [35]. In our deformed approach the situation is different, due to the role of the core in the deformed matrix element (2.5). Although we still do not have an analytical form of ISR within pn-dQRPA, it is quite remarkable that by increasing the pair basis to 200 states one obtains a small increase of the above mentioned mean ratio $\mathrm{ISR}/[3(N-Z)]$, up to 1.06. Thus, the saturation property is fulfilled within our approach. Our systematic analysis for all available deformed nuclei has shown that the Ikeda sum rule is fulfilled within 10% accuracy. For the sake of consistency in our calculations we renormalized the operators $\beta^\pm$ to exactly satisfy the Ikeda sum rule, i.e., $\beta_{\omega 0}^\pm \to \beta_{\omega 0}^\pm/\sqrt{\mathrm{ISR}}$, where by ISR we understand the summation term in Eq. (3.1).

In Fig. 3 we plot transition strengths as functions of neutron number by using the extracted $\log ft$ values defined by [35]

$$g_{\rm A}\beta_{\rm exp}^\pm = \sqrt{\frac{6147\,(2J_i+1)}{10^{\log ft}}}, \qquad (3.2)$$

where J_i is the spin of the initial nucleus and $g_{\rm A}$ denotes the effective axial-vector coupling strength. In Fig. 3 we considered an overall value $g_{\rm A} = 1$. First of all, let us take note of the overall decreasing behavior of the strengths, a feature confirmed by our calculations. On the other hand, we observe in the right panels shell effects for β^+/EC decays, more pronounced for EC transitions from even-even emitters above $N = 50$ and $N = 82$ magic numbers.

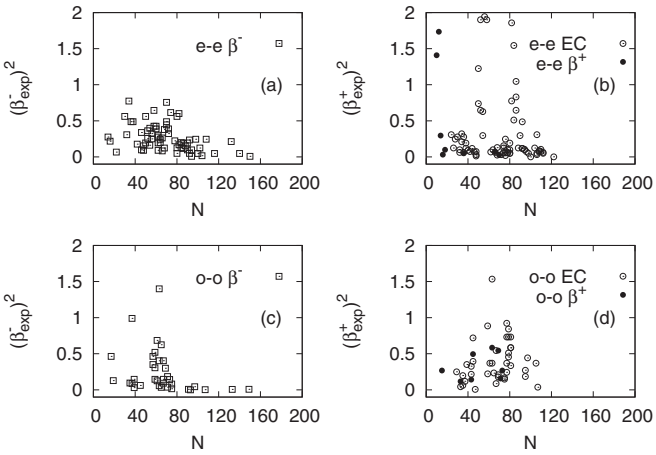

FIG. 3. Experimental transition strengths $(\beta^{\pm}_{\rm exp})^2$ versus neutron number for decays from even-even [panels (a) and (b)] and odd-odd [panels (c) and (d)] nuclei.

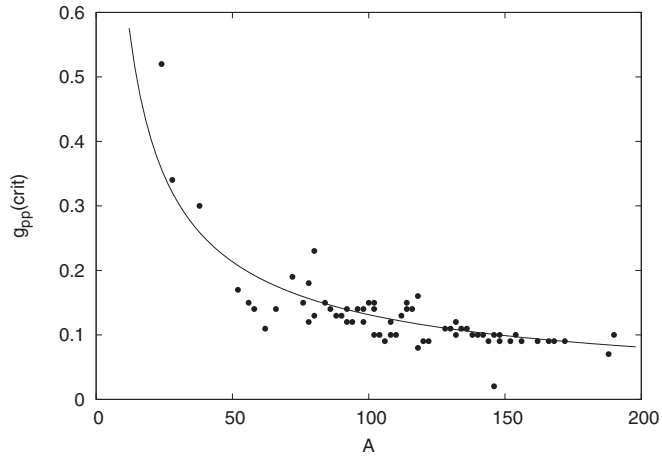

FIG. 5. Critical value of the particle-particle strength g_{pp} versus mass number. The fitting curve is $g_{\rm pp}({\rm crit}) = 3.3A^{-0.7}$.

Let us mention an interesting experimental fact, namely that similar shell effects were found for the α-decay reduced width (proportional to the spectroscopic factor) in regions close to these magic numbers [39]. The α-decay reduced width γ_0^2 used here is given by the leading monopole component, defined as

$$\Gamma = 2P_0\gamma_0^2, \tag{3.3}$$

in terms of the total α-decay width Γ and monopole penetrability through the Coulomb barrier P_0. More details can be found for example in Ref. [39], Sec. 2.5 and Eq. (2.87) contained therein.

The similar behavior of the experimental α-decay reduced width and EC transition probabilities [see panel (b) of Fig. 3] is presented in Fig. 4, where we notice the obvious linear correlations between the two mentioned quantities for transitions from even-even emitters. Large α-decay reduced widths above magic nuclei, with $100\gamma_0^2 \geqslant 1$, are explained by an enhanced α clustering in this region. For EC processes, an explanation of large peaks above magic number in Fig. 3(b), with $(\beta^{+}_{\rm exp})^2 \geqslant 0.5$, is under our further investigations, being probably connected to the fact that the few protons and neutrons above closed shells have properties similar to free nucleons.

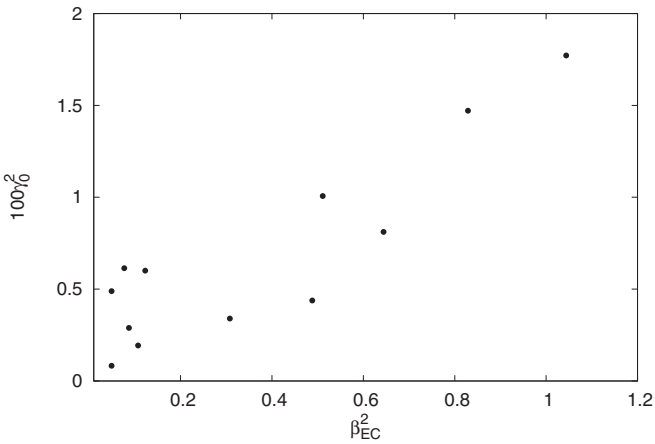

FIG. 4. The α-decay reduced width defined by Eq. (3.3) versus EC transition probability from even-even nuclei.

Our schematic approach depends on two Hamiltonian dipole parameters, namely $g_{\rm ph}$ and $g_{\rm pp}$. It is well known that the energy of the giant Gamow-Teller resonance is very sensitive to the particle-hole strength $g_{\rm ph}$. Therefore, we adjusted this parameter in order to fulfill the semiempirical rule describing the centroid of the Gamow-Teller resonance as a function of the charge and neutron numbers [35]:

$$\omega_{\rm GT} = 1.444\frac{Z+0.5}{A^{1/3}} - 30\frac{N-Z-2}{A} + 5.57. \tag{3.4}$$

The fitting line describing the above law is given by the following relation:

$$g_{\rm ph} = 0.00072A + 0.09504, \quad \sigma = 0.047. \tag{3.5}$$

Here σ is the rms deviation from the mean. It is worthwhile to note here that $g_{\rm ph}$ has very little influence on the values of the deduced effective axial-vector strengths.

Furthermore, the position of the lowest *pn* excitation described within the pn-dQRPA is sensitive to the particle-particle strength $g_{\rm pp}$. In Fig. 5 we show the critical values of this strength (where the first eigenvalue vanishes) versus the mass number. The fitting curve is given by

$$g_{\rm pp}({\rm crit}) = 3.3A^{-0.7}, \quad \sigma = 0.080. \tag{3.6}$$

Let us mention that the parameters of this curve are similar to those of Ref. [20].

Before proceeding to the comparison of the calculated and experimental β-decay rates, it is interesting to study the structure of the transition amplitudes $\beta^{\pm}$ (2.19) provided by the pn-dQRPA calculations. In Fig. 6 we present the cumulative sum for the β^- [panel (a)] and β^+ [panel (b)] type of transition amplitudes corresponding to the transitions from the 0^+ ground state of ^{78}Ge to the lowest eigenstate obtained from the pn-dQRPA diagonalization. This running

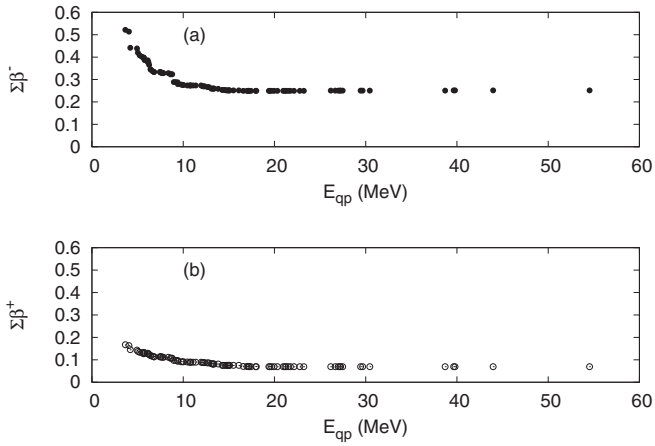

FIG. 6. Cumulative values of the β^- (a) and β^+ (b) transition matrix elements versus the quasiparticle pair energy for transitions from the 0^+ ground state of ^{78}Ge. The value $g_{pp} = 0.3g_{pp}(\text{crit})$ was adopted in the calculations.

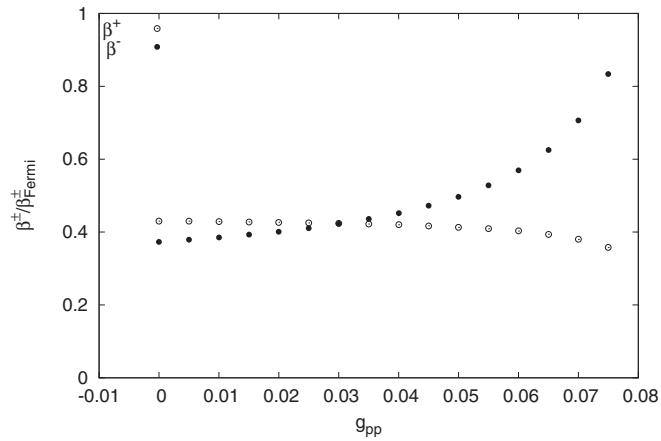

FIG. 7. Ratios $\beta^-/\beta^-_{\text{Fermi}}$ (filled circles) and $\beta^+/\beta^+_{\text{Fermi}}$ (open circles) versus g_{pp} for transitions from the 0^+ ground state of ^{78}Ge.

sum is constructed by summing over *pn* quasiparticle pairs in Eqs. (2.19) in the sequence of increasing quasiparticle pair energy $E_{qp} = E_p + E_n$. It should be noticed that the maximum value of the amplitudes corresponds to the lowest quasiparticle pair energy, i.e., to the proton and neutron single-particle states lying at the corresponding Fermi levels. The sum then decreases with increasing quasiparticle pair energy, with saturation being achieved at about half of the initial value. The explanation for this behaviour is obtained by analyzing the structure of the amplitudes given by Eq. (2.20):

It turns out that for the *pn* pair at the Fermi level (the first *pn* pair in the running sum) the first pn-dQRPA eigenvalue satisfies the condition $\omega_1 > E_p + E_n$, while for all the other *pn* pairs one has $\omega_1 < E_p + E_n$ and therefore the sign of the X amplitudes corresponding to these pairs is different from that of the first pair. Thus, the final value of the total collective transition amplitude $\beta^\pm$ is less (in this case about half) than its maximal value $\beta^\pm_{\text{Fermi}}$, given by the *pn* pair of quasiparticles corresponding to the single-particle states lying closest to the respective Fermi levels. In this analysis we used a value $g_{pp} = 0.3g_{pp}(\text{crit})$. As can be seen later from Fig. 8, the final value of the ratio $\beta^\pm/\beta^\pm_{Fermi}$ decreases from around 1 to about 0.1, by increasing the mass number.

In order to make evident the impact of the value of g_{pp} on the results presented in Fig. 6, we analyze the effects of collectivity by plotting in Fig. 7 the ratios $\beta^\pm/\beta^\pm_{\text{Fermi}}$ as functions of g_{pp} for transitions from ^{78}Ge. Here, as before, the quantity $\beta^\pm_{\text{Fermi}}$ refers to the Fermi-surface *pn* pair term of the sums of Eq. (2.19), while $\beta^\pm$ refers to the total sum. When approaching the critical value of g_{pp}, one sees an increase (decrease) of this ratio for the β^- (β^+) transitions. These changes are related to the increase in the collectivity of the lowest pn-dQRPA eigenstates.

In Fig. 8 we plot the ratios $\beta^\pm/\beta^\pm_{\text{Fermi}}$ for β^- and β^+ transitions as functions of mass number using $g_{pp} = 0.3g_{pp}(\text{crit})$. The collectivity of the transition amplitudes increases with increasing mass number, revealed by a strong and approximately linear decrease for both β^- and β^+ decays versus the mass number A. As can be seen in the figure, the *pn* pair at the Fermi surface contributes from roughly 80% to approximatively 10% in the structure of the collective transition amplitude. Thus, one can conclude that the structure of ground states in light odd-odd nuclei is mainly given by the the *pn* pair having the smallest quasiparticle energy, and corresponding to proton and neutron orbitals closest to the proton and neutron Fermi levels.

Next, we extract the effective axial-vector strength reproducing the experimental value of the transition matrix element (3.2). First of all, let us stress that its value is sensitive to the value of the particle-particle strength. This is demonstrated in Fig. 9, where we plot the dependence of g_A as function of g_{pp} for β^- (filled circles) and β^+ transitions (open circles) in the case of transitions from ^{78}Ge. We notice an interesting correlation of these plots to the dependencies in Fig. 7, defining the collectivity of the corresponding transition amplitudes $\beta^\pm/\beta^\pm_{\text{Fermi}}$.

After these preparatory studies we perform a systematic analysis of the effective value of g_A versus the mass num-

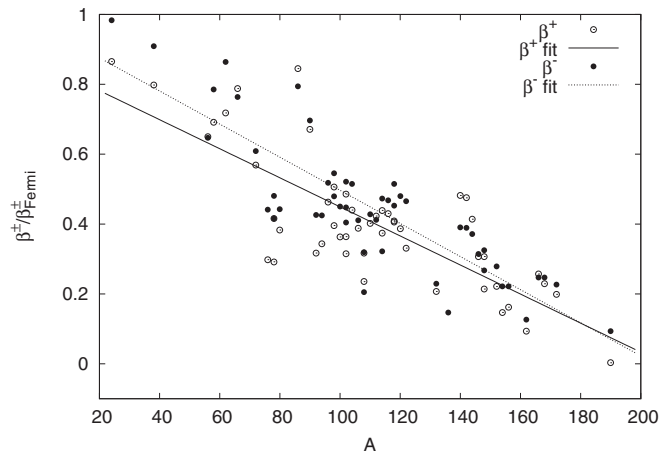

FIG. 8. Ratios $\beta^-/\beta^-_{\text{Fermi}}$ (filled circles) and $\beta^+/\beta^+_{\text{Fermi}}$ (open circles) versus mass number for $g_{pp} = 0.3g_{pp}(\text{crit})$. The corresponding dashed (solid) fitting lines are drawn to guide the eye.

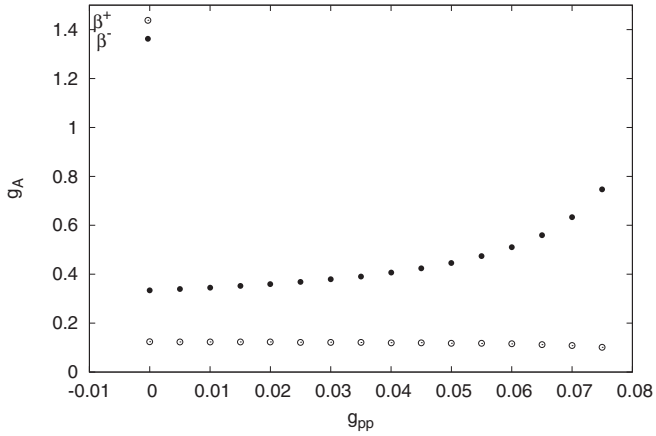

FIG. 9. Effective axial-vector strength versus the particle-particle strength in the case of ^{78}Ge for β^- (filled circles) and β^+ transitions (open circles). The $g_{\rm ph}$ values obtained from Eq. (3.5) were used.

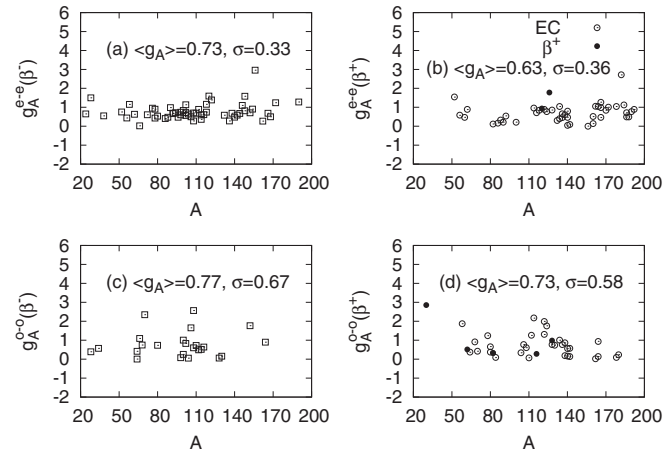

FIG. 10. Effective axial-vector strength versus the mass number A for even-even [panels (a) and (b)] and odd-odd emitters [panels (c) and (d)] for $g_{\rm pp} = 0.3 g_{\rm pp}({\rm crit})$. The averaged values with their rms deviations are given in each panel.

ber for β^- and β^+/EC transitions from (to) 0^+ ground states of even-even nuclei to (from) 1^+ ground states of the corresponding neighboring odd-odd nuclei. We exclude the emitters close to magic nucleon numbers, which are connected to anomalously large EC decay rates as discussed in the context of Fig. 3, panels (b) and (d). In the first approach we consider a constant value of $g_{\rm pp}$, while in the second iteration we fix a given ratio

$$x_g = \frac{g_{\rm pp}}{g_{\rm pp}({\rm crit})} \tag{3.7}$$

for all nuclei. It turns out that the former predicts a noticeable increase in the effective value of $g_{\rm A}$ as a function of the mass number, while in the latter we obtain a quasiconstant dependence of $g_{\rm A}$ on mass number, leading to a sensible overall mean value of this parameter. To get hold of this mean value we analyzed $\beta^{\pm}: 0^+ \to 1^+$ and $\beta^{\pm}: 1^+ \to 0^+$ transitions by changing the ratio x_g. In Fig. 10 we give a typical example for transitions from even-even nuclei [panels (a) and (b)] and odd-odd nuclei [panels (c) and (d)], corresponding to $x_g = 0.3$. One notices that the transitions from even-even nuclei provide less scattered values of $g_{\rm A}$ ($\sigma \approx 0.3$) than from odd-odd emitters ($\sigma \approx 0.6$).

The averaged values $\langle g_{\rm A} \rangle$ versus x_g for all four cases (a)–(d) in Fig. 10 are plotted in Fig. 11, panel (a), with different symbols. This dependence reveals a clear increase of the averaged axial-vector strength from $\langle g_{\rm A} \rangle \approx 0.4$ for $x_g = 0$ up to $\langle g_{\rm A} \rangle \approx 1.5$ for $x_g = 0.5$. In order to decide which is the best value of the ratio x_g we studied also the available experimental data on $2\nu\beta\beta$-decay half-lives, namely the data of Refs. [30,40]. Our calculations show that the overall mean ratio between theoretical predictions and experimental data on the $2\nu\beta\beta$-decay half-lives is rather close to unity, but the minimum of the standard rms deviation describing such transitions is achieved for $x_g = 0.3$, as can be deduced from Fig. 11, panel (b). This approach then provides a mean value of the effective axial-vector coupling $\langle g_{\rm A} \rangle = 0.68$.

References [15,16] offer a detailed survey of the effective axial-vector strength in β decay. In particular, Table 1 found in Ref. [15] gives an overview of effective $g_{\rm A}$ values taken from the literature, for various approaches. The result obtained from our calculation is in very good agreement with the listing contained there. Pairs of single-β-decaying nuclei in the mass region of $A = 100$–136 were studied in Ref. [41] in order to extract information regarding the values of the effective axial-vector strength. The many body framework was that of a spherical pn-QRPA in sp valence bases with Woods-Saxon-calculated single-particle energies. To a reasonable approximation, $g_{\rm A}$ was found to be a linear function of A with slightly different parametrizations around $A = 121$. It was also shown that, to a large extent, a mean value of $\langle g_{\rm A} \rangle = 0.6$ gives very similar results. A complex Markov chain Monte Carlo statistical analysis was performed on measured β transitions

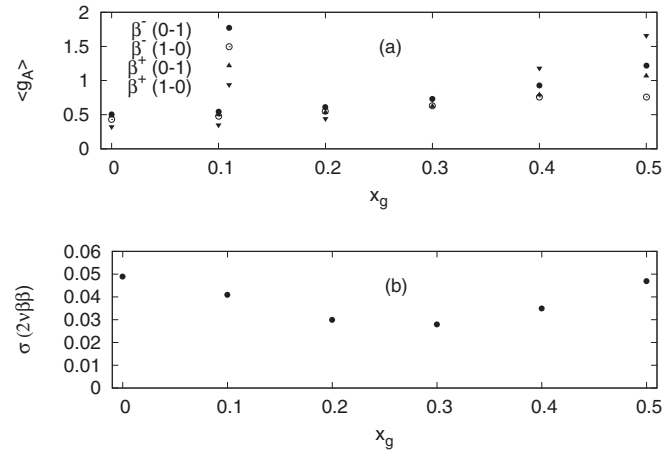

FIG. 11. (a) Averaged values of the effective axial-vector strength for the four cases in Fig. (10) versus the ratio (3.7). (b) Standard rms deviation in the $2\nu\beta\beta$-decay calculations versus the same ratio.

for the mass range $A = 62$–142, in Ref. [42]. The corresponding $\log ft$ values were compared with the theoretical ones obtained from the spherical pn-QRPA with a realistic force. The results suggested an apparent quenching of g_A in an extended analysis and also provided a realistic estimate of the parametric uncertainty inherent in the nuclear model. The average values of g_A which can be deduced from [42] are commensurate with those put forward in [41] and in this work.

We also note that the average value of g_A obtained in the present work is about twice the average computed in Ref. [31]. There, the spherical pn-QRPA was employed together with a schematic dipole interaction containing particle-particle and particle-hole parts with mass-dependent strengths. Let us also mention that this averaged value was obtained by simultaneously analyzing β^- and β^+/EC data from nine isobaric triplets, while in this paper we determined $\langle g_A \rangle$ by using a much larger sample of data.

IV. CONCLUSIONS

We analyzed the experimental Gamow-Teller β^- and β^+/EC decay rates between 0^+ ground states of even-even nuclei and 1^+ ground states in neighboring odd-odd nuclei, combined with the experimentally known $2\nu\beta\beta$ half-lives in order to derive an average effective value of the weak axial-vector strength g_A. The necessary pn-QRPA equations of motion were derived in terms of a single-particle basis with projected angular momentum provided by the diagonalization of a deformed mean field plus a schematic quadrupole-quadrupole residual interaction. The parameters involved are mass dependent particle-hole (ph) and particle-particle (pp) strengths.

Let us mention that the comparison between the pn-dQRPA in the laboratory system and the standard intrinsic approach is an important issue. For particle-hole excitations described by dQRPA [29] we already obtained some preliminary results by analyzing quadrupole electromagnetic transitions [43]. Thus, the gross features of amplitudes are very similar, but the the intrinsic $B(E2)$ values are underestimated with respect to their laboratory counterparts, due to the lack of symmetry restoration for the QRPA ground state within the intrinsic approach. We expect a similar behavior in the case of pn-dQRPA.

It turned out that the collectivity of transition amplitudes increases linearly with the increasing mass number. This behavior has an important consequence, namely that the structure of ground states in light odd-odd nuclei is mainly given by the *pn* pair occupying single-particle states closest to the Fermi level.

We also evidenced an important experimental fact: the available EC transition matrix elements are proportional to the α-decay reduced widths from even-even emitters. Our simultaneous analyses of beta decay and double-beta decay data led to a quenched average effective value $\langle g_A \rangle \approx 0.7$, with a root-mean-square deviation of $\sigma \approx 0.3$ for transitions from even-even emitters and $\sigma \approx 0.6$ for transitions from odd-odd emitters.

Let us finally mention that the effective value of g_A is also important in spin-multipole excitations [44], astrophysical applications [45,46], isoscalar pairing investigations [47], the relativistic approach [48], and the charge-exchange strength function [49].

ACKNOWLEDGMENTS

This work has been partially supported by grants of the Romanian Ministry of Research and Innovation, CNCS-UEFISCDI, PN-III-P4-ID-PCE-2016-0092, PN-III-P4-ID-PCE-2016-0792, within PNCDI III, PN-19060105/2019, and by the Academy of Finland (Suomen Akatemia) under Academy Project No. 318043.

[1] F. T. Avignone III, S. R. Elliott, and J. Engel, Rev. Mod. Phys. **80**, 481 (2008).
[2] J. Maalampi and J. Suhonen, Adv. High Energy Phys. **2013**, 505874 (2013).
[3] J. Suhonen and O. Civitarese, Phys. Rep. **300**, 123 (1998).
[4] A. Escuderos, A. Faessler, V. Rodin, and F. Šimkovic, J. Phys. G: Nucl. Part. Phys. **37**, 125108 (2010).
[5] J. Suhonen and O. Civitarese, J. Phys. G **39**, 124005 (2012).
[6] R. Sahu, P. C. Srivastava, and V. K. B. Kota, J. Phys. G: Nucl. Part. Phys. **40**, 095107 (2013).
[7] J. Engel, J. Phys. G: Nucl. Part. Phys. **42**, 034017 (2015).
[8] J. Barea, J. Kotila, and F. Iachello, Phys. Rev. C **87**, 014315 (2013).
[9] A. Juodagalvis and D. J. Dean, Phys. Rev. C **72**, 024306 (2005).
[10] E. Caurier, F. Nowacki, and A. Poves, Phys. Lett. B **711**, 62 (2012).
[11] A. Faessler, G. L. Fogli, E. Lisi, V. Rodin, A. M. Rotunno, and F. Šimkovic, J. Phys. G: Nucl. Part. Phys. **35**, 075104 (2008).
[12] J. Suhonen and O. Civitarese, Phys. Lett. B **725**, 153 (2013).
[13] N. Yoshida and F. Iachello, Prog. Theor. Exp. Phys. **2013**, 043D01 (2013).
[14] H. Ejiri, J. Suhonen, and K. Zuber, Phys. Rep. **797**, 1 (2019).
[15] J. Suhonen, Front. Phys. **5**, 55 (2017).
[16] J. Suhonen and J. Kostensalo, Front. Phys. **7**, 29 (2019).
[17] J. Suhonen and O. Civitarese, J. Phys. G: Nucl. Part. Phys. **39**, 085105 (2012).
[18] P. Sarriguren, E. Moya de Guerra, A. Escuderos, and A. C. Carrizo, Nucl. Phys. A **635**, 55 (1998).
[19] P. Sarriguren, E. Moya de Guerra, and A. Escuderos, Nucl. Phys. A **658**, 13 (1999); **691**, 631 (2001).
[20] H. Homma, E. Bender, M. Hirsch, K. Muto, H. V. Klapdor-Kleingrothaus, and T. Oda, Phys. Rev. C **54**, 2972 (1996).
[21] L. Pacearescu, V. Rodin, F. Simkovic, and A. Faessler, Phys. Rev. C **68**, 064310 (2003).
[22] F. Šimkovic, L. Pacearescu, and A. Faessler, Nucl. Phys. A **733**, 321 (2004).
[23] R. Alvarez-Rodriguez, P. Sarriguren, E. Moya de Guerra, L. Pacearescu, A. Faessler, and F. Šimkovic, Phys. Rev. C **70**, 064309 (2004).
[24] P. Sarriguren, Phys. Rev. C **86**, 034335 (2012).
[25] D. D. Ni and Z. Z. Ren, J. Phys. G: Nucl. Part. Phys. **41**, 125102 (2014).

[26] A. A. Raduta, D. S. Delion, and N. Lo Iudice, Nucl. Phys. A **551**, 93 (1993).
[27] A. A. Raduta, D. S. Delion, and A. Faessler, Phys. Lett. B **312**, 13 (1993).
[28] A. A. Raduta, A. Escuderos, A. Faessler, E. Moya de Guerra, and P. Sarriguren, Phys. Rev. C **69**, 064321 (2004).
[29] D. S. Delion and J. Suhonen, Phys. Rev. C **87**, 024309 (2013).
[30] D. S. Delion and J. Suhonen, Phys. Rev. C **95**, 034330 (2017).
[31] D. S. Delion and J. Suhonen, Europhys. Lett. **107**, 52001 (2014).
[32] D. S. Delion and J. Suhonen, Phys. Rev. C **91**, 054329 (2015).
[33] O. Civitarese and J. Suhonen, J. Phys. G: Nucl. Part. Phys. **20**, 1441 (1994).
[34] O. Civitarese and J. Suhonen, Nucl. Phys. A **578**, 62 (1994).
[35] J. Suhonen, *From Nucleons to Nucleus: Concepts of Microscopic Nuclear Theory* (Springer, Berlin, 2007).
[36] P. Singh, L. J. Rodriguez, S. S. M. Wong, and J. K. Tuli, Nucl. Data Sheets **84**, 487 (1998).
[37] J. Dudek, W. Nazarewicz, and T. Werner, Nucl. Phys. A **341**, 253 (1980).
[38] P. Möller and J. R. Nix, Nucl. Phys. A **272**, 502 (1995).
[39] D. S. Delion, *Theory of Particle and Cluster Emission* (Springer, Berlin, 2010).
[40] A. S. Barabash, in *Workshop on Calculation of Double-Beta-Decay Matrix Elements (MEDEX '13), June 2013, Prague*, edited by O. Civitarese, I. Stekl, and J. Suhonen, AIP Conf. Proc. No. 1572 (AIP, New York, 2013), p. 11.
[41] P. Pirinen and J. Suhonen, Phys. Rev. C **91**, 054309 (2015).
[42] F. F. Deppisch and J. Suhonen, Phys. Rev. C **94**, 055501 (2016).
[43] F.-Q. Chen, D. S. Delion, and Y. Niu (unpublished).
[44] J. Kostensalo and J. Suhonen, Phys. Rev. C **95**, 014322 (2017).
[45] T. Marketin, L. Huther, and G. Martinez-Pinedo, Phys. Rev. C **93**, 025805 (2016).
[46] Z. M. Niu, Y. F. Niu, H. Z. Liang, W. H. Long, T. Nikčic, D. Vretenar, and J. Meng, Phys. Lett. B **723**, 172 (2013).
[47] Z. M. Niu, Y. F. Niu, Q. Liu, H. Z. Liang, and J. Y. Guo, Phys. Rev. C **87**, 051303(R) (2013).
[48] C. Robin and E. Litvinova, Phys. Rev. C **98**, 051301(R) (2018).
[49] J. Terasaki, Phys. Rev. C **97**, 034304 (2018).